Since January 2020 Elsevier has created a COVID-19 resource centre with free information in English and Mandarin on the novel coronavirus COVID-19. The COVID-19 resource centre is hosted on Elsevier Connect, the company's public news and information website.

Elsevier hereby grants permission to make all its COVID-19-related research that is available on the COVID-19 resource centre - including this research content - immediately available in PubMed Central and other publicly funded repositories, such as the WHO COVID database with rights for unrestricted research re-use and analyses in any form or by any means with acknowledgement of the original source. These permissions are granted for free by Elsevier for as long as the COVID-19 resource centre remains active.

Bioorg. Med. Chem. Lett. 66 (2022) 128732

Contents lists available at ScienceDirect

Bioorganic & Medicinal Chemistry Letters

journal homepage: www.elsevier.com/locate/bmcl

Identification of *Aloe*-derived natural products as prospective lead scaffolds for SARS-CoV-2 main protease (M^{pro}) inhibitors

Emily G. Hicks, Sylvie E. Kandel, Jed N. Lampe [*]

Department of Pharmaceutical Sciences, Skaggs School of Pharmacy, University of Colorado, Aurora, CO 80045, United States

ARTICLE INFO

Keywords:
SARS-CoV-2 main protease
M^{pro}
$3CL^{pro}$
Aloe
Natural products
Aloesin
aloeresin D
Protease inhibitors

ABSTRACT

In the past two years, the COVID-19 pandemic has caused over 5 million deaths and 250 million infections worldwide. Despite successful vaccination efforts and emergency approval of small molecule therapies, a diverse range of antivirals is still needed to combat the inevitable resistance that will arise from new SARS-CoV-2 variants. The main protease of SARS-CoV-2 (M^{pro}) is an attractive drug target due to the clinical success of protease inhibitors against other viruses, such as HIV and HCV. However, in order to combat resistance, various chemical scaffolds need to be identified that have the potential to be developed into potent inhibitors. To this end, we screened a high-content protease inhibitor library against M^{pro} *in vitro*, in order to identify structurally diverse compounds that could be further developed into antiviral leads. Our high-content screening efforts retrieved 27 hits each with $>$ 50% inhibition in our M^{pro} FRET assay. Of these, four of the top inhibitor compounds were chosen for follow-up due to their potency and drugability (Lipinski's rules of five criteria): anacardic acid, aloesin, aloeresin D, and TCID. Further analysis via dose response curves revealed IC_{50} values of 6.8 μM, 38.9 μM, 125.3 μM, and 138.0 μM for each compound, respectively. Molecular docking studies demonstrated that the four inhibitors bound at the catalytic active site of M^{pro} with varying binding energies (-7.5 to −5.6 kcal/mol). Furthermore, M^{pro} FRET assay kinetic studies demonstrated that M^{pro} catalysis is better represented by a sigmoidal Hill model than the standard Michaelis-Menten hyperbola, indicating substantial cooperativity of the active enzyme dimer. This result suggests that the dimerization interface could be an attractive target for allosteric inhibitors. In conclusion, we identified two closely-related natural product compounds from the *Aloe* plant (aloesin and aloeresin D) that may serve as novel scaffolds for M^{pro} inhibitor design and additionally confirmed the strongly cooperative kinetics of M^{pro} proteolysis. These results further advance our knowledge of structure–function relationships in M^{pro} and offer new molecular scaffolds for inhibitor design.

The global scourge of the COVID-19 pandemic has enveloped the world for two years, leaving over 5 million dead and 250 million infected in its wake.[1–2] Despite the emerging success of vaccines, a significant number of people remain unvaccinated, either due to lack of availability[3] or vaccine hesitancy.[4–5] Furthermore, "breakthrough" infections are becoming more common in the vaccinated with the identification of new variants,[6–7] leaving few therapeutic options available for life threatening infections.[8–9] This illustrates the need to develop novel small molecule chemical modalities that can be used both to treat severe SARS-CoV-2 infections and as potential prophylactic agents in high-risk population groups. While the earliest small molecule therapies targeting SARS-CoV-2 directed their activities towards the RNA polymerase target (e.g., remdesivir and molnupiravir), recent attention has turned to the 3C-like viral main protease ($3CL^{pro}$ or M^{pro}) as a possible drug target.[10–17] Viral protease inhibitors have previously demonstrated high clinical efficacy against other viruses, such as HIV (human immunodeficiency virus)[18–19] and HCV (hepatitis C virus),[20–22] making M^{pro} an attractive target for antiviral drug development. Indeed, Pfizer, Inc. has a first-in-class M^{pro} inhibitor currently in Phase III clinical trials,[11] pointing to M^{pro} inhibition as an effective therapeutic strategy. Despite this, a major liability of viral protease inhibitors is the eventual development of resistance, which necessitates their use as part of combination therapy and also the development of second and third generation compounds. This highlights the need for the identification of new lead structures that may function as M^{pro} inhibitor scaffolds.[12,14–15] Since the publication of the SARS-CoV-2 M^{pro} crystal structure,[23] a number of campaigns have been conducted to identify selective M^{pro} inhibitors[11–12,14–16,23–29] While most of these published accounts have

---

[*] Corresponding author.
E-mail address: jed.lampe@cuanschutz.edu (J.N. Lampe).

https://doi.org/10.1016/j.bmcl.2022.128732
Received 9 December 2021; Received in revised form 31 March 2022; Accepted 8 April 2022
Available online 12 April 2022
0960-894X/© 2022 Elsevier Ltd. All rights reserved.

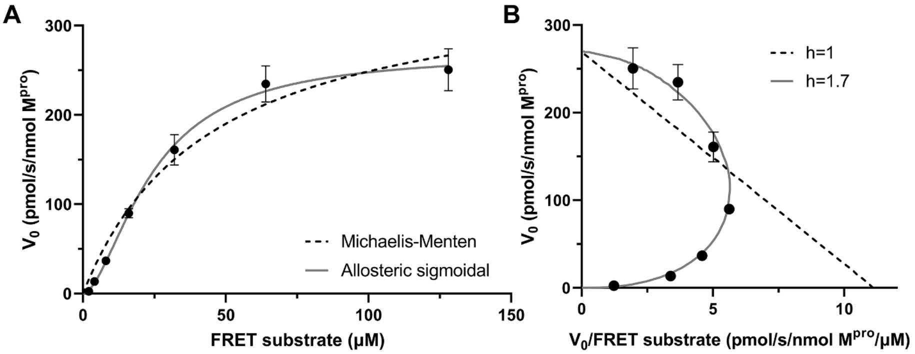

Fig. 1. Kinetic analysis of FRET substrate proteolysis by M^{pro}. A: Kinetic data fit to Michaelis-Menten and allosteric sigmoidal (Hill) models. B: Eadie-Hofstee transformation of Hill equation at h = 1 (no cooperativity) and h = 1.7 (positive cooperativity). The kinetic assay was performed at 2–128 μM FRET substrate and 100 nM M^{pro}. Initial velocities in RFU converted to pmol/s with the free Edans calibration curve. Points represent mean of triplicate measurements ± standard deviation.

exclusively involved computational approaches,[16,25,26,30] several have screened existing small molecule libraries for M^{pro} inhibition *in vitro*.[13,15,31] However, these approaches have led to a number of redundant hits with similar mechanisms of action.[32–34] In order to forestall eventual viral resistance, chemical diversity is an important consideration in identification of early protease inhibitor leads.[35–39] Even small chemical libraries that are highly diverse can lead to the identification of inhibitors with unique mechanisms of action.[40–42] In an attempt to expand the chemical diversity of potential scaffolds for SARS-CoV-2 M^{pro} inhibitor lead design, our approach focused on a high-content protease inhibitor library to filter out redundant molecules and obtain unique pharmacophores that could be further exploited by chemical optimization. Here, we report the identification of novel *Aloe*-derived natural product scaffolds that have the potential to be further optimized into effective clinical candidates, given their high drug-like qualities (Lipinski's rule of five [43,44]) and safety profiles. Additionally, our data confirm that SARS-CoV-2 M^{pro} functions as a cooperative dimer, hinting at the possibility of developing allosteric inhibitors that may target and disrupt the enzyme dimer interface.

In order to screen library compounds for inhibitory activity against M^{pro} in an *in vitro* system, we cloned, expressed, and purified the M^{pro} viral protein in an *E. coli* based heterologous expression system.[45] To facilitate production of the native protease, we retained the original viral *N*-terminal autocatalytic cleavage site (SAVLQ↓SGFRK) and modified the C-terminal sequence with the core amino acids of the HRV (human rhinovirus)–3C protease cleavage site (VTFQ↓GP) to permit removal of the His tag needed for the protein purification (see supporting information, Figure S1). This construct resulted in high yields of the native protein (see supporting information, Figure S2). To ascertain proteolytic activity, we relied on a FRET (fluorescence resonance energy transfer)-based assay with the peptide substrate Dabcyl-KTSAVLQ↓SGFRKME-Edans-NH_2, which emits a fluorescent signal at 460 nm when cleaved and excited at 360 nm.[46] Once we evaluated our M^{pro} activity assay for linearity as a function of time and protein concentration (see supporting information, Figure S3), a kinetic experiment was performed at 100 nM M^{pro}, 2–128 μM FRET substrate (5% final volume dimethyl sulfoxide, DMSO) in 100 μL final reaction volume with reaction buffer comprised of 20 mM Tris HCl, 100 mM NaCl, 1 mM EDTA, 1 mM DTT, pH 7.3 at 37 °C. The reaction was initiated by adding 50 μL of the FRET substrate in reaction buffer to 50 μL of M^{pro} in reaction buffer. Cleavage of the substrate was measured via fluorescence on a Tecan Infinite M Plex plate reader every minute for 30 min. A free Edans calibration curve from 0.1 to 25 μM was used to convert the initial velocities in RFU (relative fluorescence units) to pmol/s. Concentration of FRET substrate vs. initial velocity was plotted (Fig. 1) and analyzed for kinetic parameters via GraphPad Prism (v. 9.2.0.332). Both Michaelis-Menten and allosteric sigmoidal models (Hill equation) were assessed (Fig. 1A) and compared via the second order Akaike Information Criterion (AICc).[47] The resulting kinetic parameters for the Michaelis-Menten fit were $K_m = 44.6 \pm 8.0$ μM and $V_{max} = 359.6 \pm 27.8$ pmol/

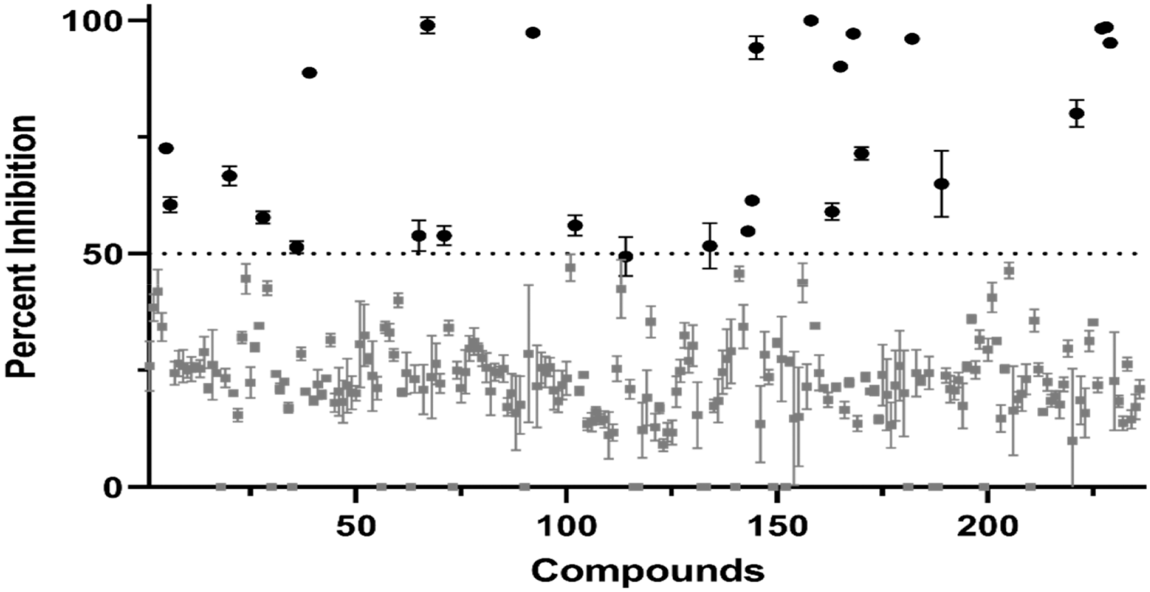

Fig. 2. High-content library screening for M^{pro} inhibition. A total of 236 protease inhibitors were screened at 100 μM against M^{pro}. Hits are defined as compounds with over 50% inhibition, represented by black circles. Compounds with less than 50% inhibition are represented by gray squares. Percent inhibition was calculated against DMSO control. Data points represent the mean of three replicates ± standard deviation (several standard deviations are too small to be discernable).

Table 1
M^{pro} inhibitors identified from high content protease inhibitor library screening.

Compound	Structure	Inhibition (%)	Compound	Structure	Inhibition (%)	Compound	Structure	Inhibition (%)
Z-DEVD-FMK	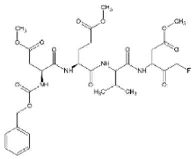	100.0 ± 0.7	Z-FA-FMK	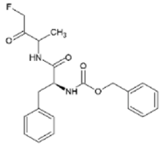	90.1 ± 0.8	Leupeptin hemisulfate	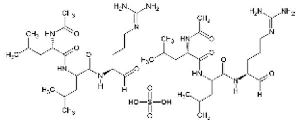	59.0 ± 1.8
Calpain Inhibitor II	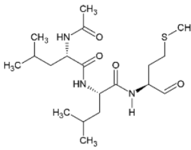	99.8 ± 0.7	Telaprevir	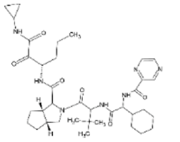	88.8 ± 0.5	Celastrol	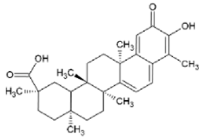	57.7 ± 1.3
MG-132	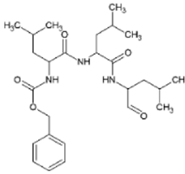	99.0 ± 1.7	Aloesin [a] (aloeresin B)	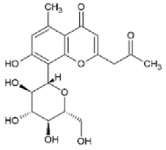	80.1 ± 2.9	Nelfinavir mesylate	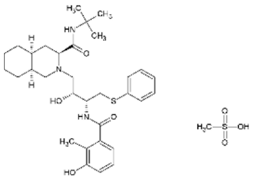	56.1 ± 2.2
Calpain Inhibitor XII	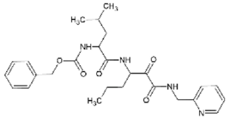	98.3 ± 0.3	Aloeresin D [a]	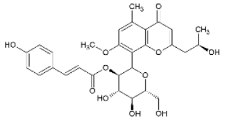	72.6 ± 1.1	IU1	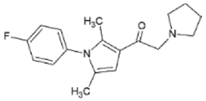	54.8 ± 0.1
Boceprevir	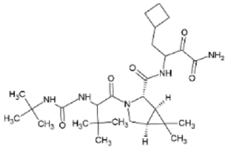	97.4 ± 0.2	PD 151,746	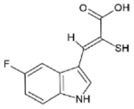	71.5 ± 1.4	Tanshinone IIA [a]	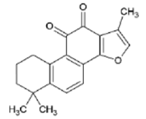	53.9 ± 3.3
Calpeptin	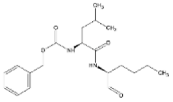	97.2 ± 0.1	Mocetinostat [a]	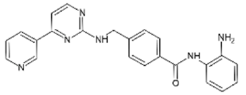	66.7 ± 2.1	Dibenzazepine	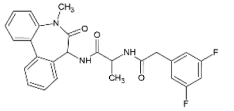	53.8 ± 2.0
Anacardic acid	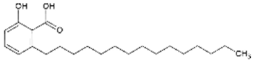	96.1 ± 0.1	L-685,458	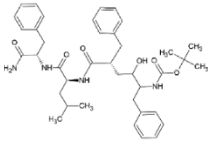	65.0 ± 7.1	Glecaprevir [a]	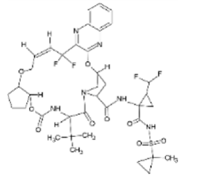	51.7 ± 4.9
Calpain Inhibitor I (MG-101)	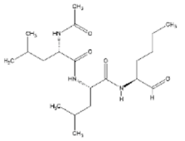	95.2 ± 0.9	LDN-57444	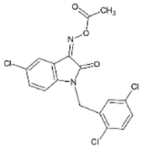	61.4 ± 1.0	MC1568	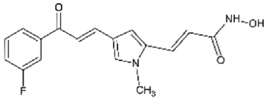	51.4 ± 1.3
TCID [a]	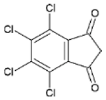	94.2 ± 2.5	7-O-Methyl- aloeresin A	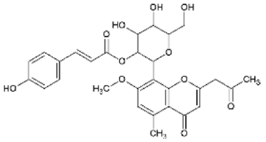	60.5 ± 1.7	Asunaprevir [a]	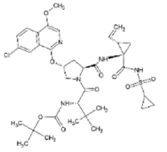	49.4 ± 4.2

Percent inhibition values represent mean of three replicates ± standard deviation. [a] Compound with background fluorescence.

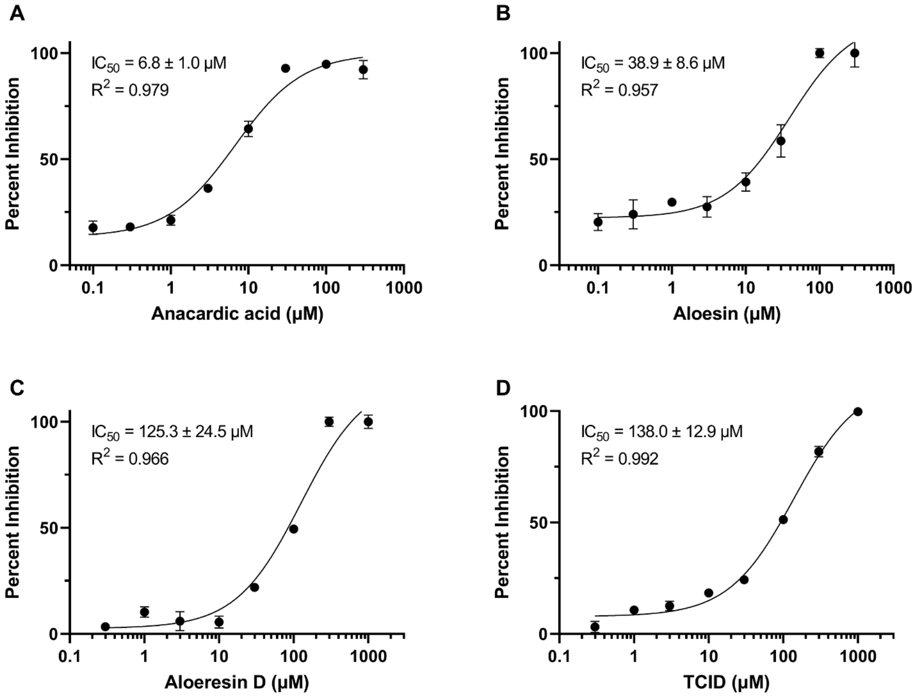

Fig. 3. Dose response curves of anacardic acid (A), aloesin (B), aloeresin D (C), and TCID (D) against M^{pro}. Percent inhibition calculated against the DMSO control and analyzed in GraphPad Prism via non-linear regression with a dose–response inhibition model (three parameters). Points represent mean of triplicates ± standard deviation (several standard deviations are too small to be discernable).

S/Nmol M^{pro}, and $S_{50} = 24.2 \pm 2.0$ μM and $V_{max} = 269.6 \pm 11.4$ pmol/S/Nmol M^{pro} for the allosteric sigmoidal fit (see supporting information, Table S1).

Interestingly, the data best fit to the sigmoidal Hill plot with an R^2 of 0.985 and an AICc correct fit probability of 99.98%. This is dramatically apparent when the data is analyzed by the Eadie-Hofstee transformation (Fig. 1B). The presence of cooperativity in enzyme activity is readily explainable and somewhat expected as the enzyme is reported to be only active as a dimer.[48–50] However, while allosteric cooperativity has been demonstrated previously for this enzyme,[51–53] this is the first time that kinetic data have been quantitatively compared to determine the best model for enzyme activity, i.e. either the Michaelis-Menten or the sigmoidal Hill equations (Fig. 1A, Table S1). The clear appearance of allosteric kinetics, as represented in the Eadie-Hofstee plot (Fig. 1B), indicates that the allosteric dimer interface may also be a promising inhibitor target, as was found to be the case for the SARS-CoV-1 M^{pro} enzyme.[50]

For our high-content library screening, a total of 236 compounds were obtained from different vendors: Protease Inhibitor Library (catalog no. L2500) and PF-00835231 from Selleck Chemicals (Houston, TX); ebselen from Sigma-Aldrich (St. Louis, MO); aloin B, aloe-emodin, calpain inhibitor II, calpain inhibitor III, calpain inhibitor VI, calpain inhibitor XII, 2-cyano-pyrimidine, E-64d, oseltamivir (phosphate), PD 150606, PSI-7977, tosyllysine chloromethyl ketone HCl, and pimodivir from Cayman Chemical (Ann Arbor, MI); aloeresin D from eNovation Chemicals (Green Brook, NJ); and 7-*O*-methylaloeresin A from Muse Chem (Fairfield, NJ). The inhibition screening assays were performed at 50 nM M^{pro}, 10 μM FRET substrate, and 100 μM inhibitor (1.5% final volume DMSO). 100 μM inhibitor concentration was selected as our goal was not to identify highly potent compounds, but rather chemically diverse leads. The Pfizer M^{pro} inhibitor, PF–00835231, was used as a positive control for inhibition at a concentration of 1 μM. The reactions were initialized at room temperature by the addition of 50 μL FRET substrate and inhibitor mixture, dissolved in reaction buffer, to 50 μL of M^{pro} also prepared in reaction buffer. The reaction buffer consisted of 20 mM Tris HCl, 100 mM NaCl, 1 mM EDTA, and 1 mM DTT, pH 7.3 at room temperature. Fluorescence was monitored for 1 h, with readings taken every 2.5 min. The first 20 min were used to calculate the initial velocity, and percent inhibition was calculated from the slope compared to the DMSO control. Background from the FRET substrate was subtracted from all samples. All experiments were performed in triplicate and the presented values represent the mean ± standard deviation. Positive "hits" were defined as any compound that inhibited M^{pro} activity by 50% or more. As can be seen in Fig. 2, 27 compounds fell into this category, indicating an assay hit rate of approximately 11.4%. The structures and percent inhibition are shown in Table 1, demonstrating the chemical diversity present in the hits obtained from the initial library screening. To assess assay robustness, the Z'-factor was calculated for each screening experiment (see supporting information, Figure S4). The resulting Z'-factors were between 0.727 and 0.969, well within the guidelines of 0.5 to 1 for a high-throughput assay.[54]

Inherent limitations of the FRET-based assay led to 19 of the initial library compounds (8.1%) being eliminated from the assay screen due to either intrinsic fluorescence from the compounds themselves or issues stemming from inner filter effects. Some of the compounds we identified have been previously reported as SARS-CoV-2 M^{pro} inhibitors (see supporting information, Table S2), thereby increasing our confidence in the robustness of our M^{pro} screening assay. Interestingly, a number of the most potent compounds are natural products (e.g., anacardic acid, aloesin, aloeresin D).

Aloesin and aloeresin D come from the *Aloe* plant, including *Aloe perryi* and *A. barbadensis* (aka, *A. vera*) species.[55–56] These compounds have a long history of medicinal use as stimulant-laxatives to treat constipation,[57] anti-inflammatory compounds to promote wound healing,[58] and bittering agents in food supplements, thereby demonstrating their positive safety profile and bioavailability in humans.[56] Furthermore, aloesin is a known tyrosinase inhibitor with an IC_{50} of 0.9 mM against mushroom tyrosinase.[59–60] Anacardic acid is a natural product from the cashew nut that exhibits anti-inflammatory and antinociceptive properties.[61]Due to the chemical novelty of the natural products identified and the availability of readily accessible functional groups on these compounds for further modification, we decided to

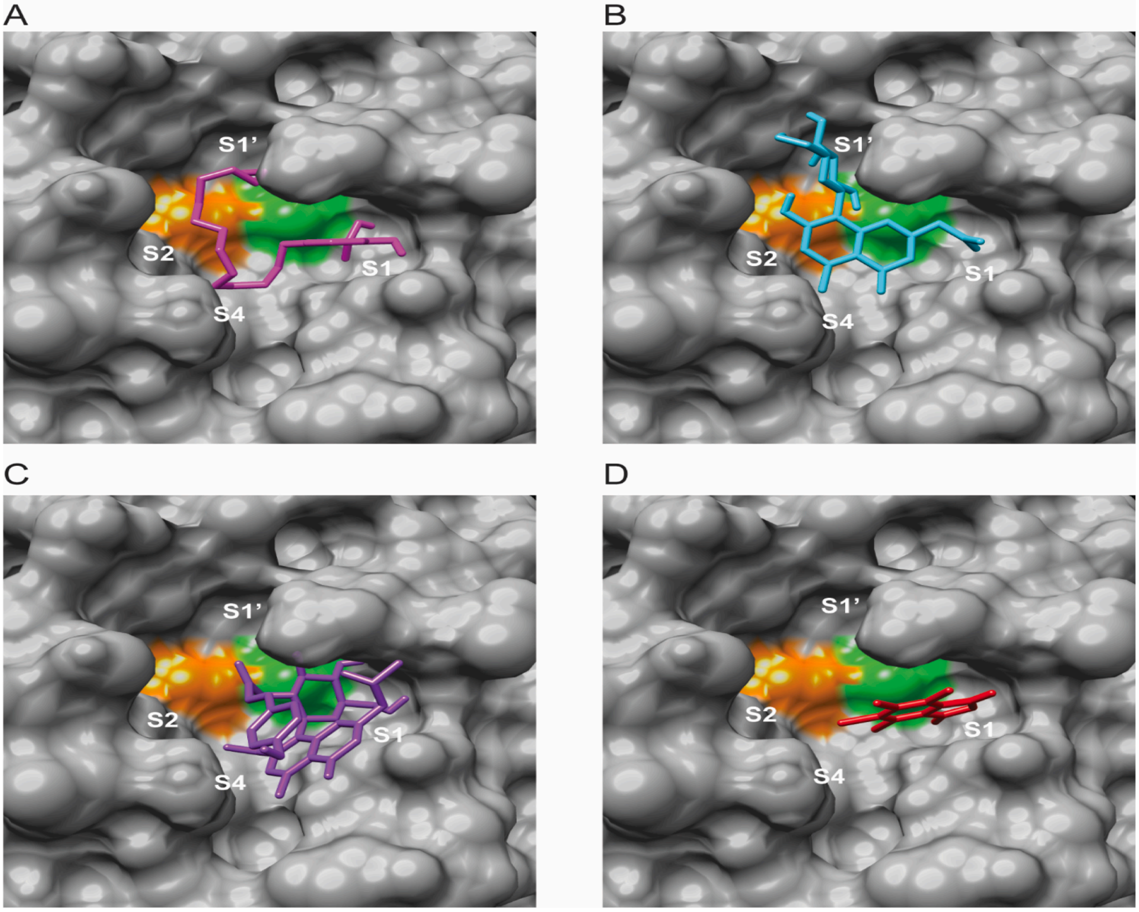

Fig. 4. Docking of anacardic acid, aloesin, aloeresin D, and TCID in M^{pro} active site. A. Anacardic acid (magenta) docked with a predicted affinity of −5.6 kcal/mol. B. Aloesin (cyan) docked with a predicted affinity of −7.5 kcal/mol. C. Aloeresin D (purple) docked with a predicted affinity of −6.8 kcal/mol. D. TCID (red) docked with a predicted affinity of −5.8 kcal/mol. The catalytic dyad of Cys 145 and His 41 are displayed in green and orange respectively. (For interpretation of the references to colour in this figure legend, the reader is referred to the web version of this article.)

focus on the top three natural products with high percent inhibition in the 100 μM screen: anacardic acid (96.1% ± 0.1), aloesin (80.1% ± 2.9), and aloeresin D (72.6% ± 1.1).

We also chose to include the non-natural product TCID (a selective ubiquitin C-terminal hydrolase-L3 inhibitor), due to its performance in the high-content screen (94.2% ± 2.5).[62] In order to quantitatively assess the extent of M^{pro} inhibition, we performed IC_{50} experiments using the screening assay that we had already developed. The dose response curves in Fig. 3 demonstrate IC_{50}′s in the micromolar range. It should be noted that 0% inhibition (100% activity) was not reached in all cases due to assay background fluorescence.

TCID (IC_{50} = 138.0 μM ± 12.9), was ruled out as a possible scaffold due to its higher IC_{50} value and potential toxicity.[63] While the most potent inhibitory compound was anacardic acid (IC_{50} = 6.8 μM ± 1.0), its toxic liabilities may also prevent it from further development as an antiviral agent, whereas the two *Aloe* compounds (aloesin IC_{50} = 38.9 μM ± 8.6, aloeresin D IC_{50} = 125.3 μM ± 24.5), have a more favorable safety and efficacy profile in humans.[56] The four hits were also pre-incubated with and without the enzyme in order to assess time-dependent inhibition (TDI) (see supporting information, Figure S5). While a single inhibitor concentration is not conclusive, the data suggest that the compounds exhibit a moderate amount of TDI. Experiments involving multiple concentrations points will need to be carried out to further delineate the TDI potential of these compounds.

Table S3 (see supporting information) illustrates Lipinski's rule of five for the four inhibitors: aloesin and TCID meet all four criteria, while anacardic acid and aloeresin D have one and two violations respectively. Compounds meeting at least three of the four of Lipinski's criteria generally make excellent orally active drugs.[43–44]

In an effort to expand our knowledge as to the specific mode of action of these compounds, a molecular docking study was undertaken using the AutoDock Vina algorithm, v. 1.1.2.[64] Briefly, the SARS-CoV-2 M^{pro} crystal structure (PDB entry 6Y2E) was prepared for docking by removing ions and water molecules and adding polar hydrogens using MGL AutoDock Tools v. 1.5.7 (UCSD Molecular Graphics Lab and The Scripps Research Institute). Inhibitor (PF-00835231, anacardic acid, aloesin, aloeresin D, and TCID) structural coordinates were obtained from the Protein Data Bank (PDB: https://www.rcsb.org/) and parameterized by adding polar hydrogens and identifying rotatable bonds. The receptor docking grid was defined by the following parameters - grid box center: x-center = -16.022, y-center = –32.73, z-center = 4.648, and the total number of grid points in each dimension being: x-dimension = 80, y-dimension = 48, and z-dimension = 62. To facilitate an efficient docking routine, a configuration file docking script was prepared using MS Notepad in simple text format with the energy range set to 4 and the exhaustiveness search parameter set to 24. AutoDock Vina was executed using the configuration file with both PDBQT.out and log.out file options selected. The PDBQT.out file contains all of the ligand binding poses for any particular docking simulation. Output files were analyzed using the ViewDock function of UCSF Chimera v.1.15, and ranked according to binding energy (ΔG). To test the validity of AutoDock Vina to predict the correct binding pose for our selected inhibitors, we first attempted to dock PF-00835231 using the parameters described above. The reported IC_{50} of Pfizer's reference inhibitor is in the low nanomolar range (6.9 nM). Here, we found that the lower IC_{50} value correlated with the lower docking score, both indicating higher affinity for the enzyme. The most energetically stable pose found the compound bound in the active site within close proximity of the catalytic dyad (Cys 145 and His 41) (see supporting information, Figure S6). This docking pose is strikingly similar, although not quite superimposable, with the location of the compound found in PDB entry 6HXM, where it is covalently adducted to Cys 145. The difference in position is likely due to the covalent adduct formed between PF00835231 and Cys 145 during catalysis.

As seen in Fig. 4, all four inhibitors docked within the active site of M^{pro}, near the catalytic dyad of Cys 145 and His 41, although with differing binding energies. Aloesin bound with the lowest predicted free energy, −7.5 kcal/mol, followed by aloeresin D at −6.8 kcal/mol, TCID at −5.8 kcal/mol, and anacardic acid at −5.6 kcal/mol. TCID, the smallest molecule, docked near the Cys 145 at subsite S1 (Fig. 4D). Both aloesin and anacardic acid are bound in extended conformations, occupying the entirety of the active site, including subsites S1, S1′, S2, and S4 (Fig. 4 A, B). In contrast, aloeresin D (Fig. 4C) is bound in the active site in a more sterically constrained conformation, with the vinylphenol ring hovering just above the glycosyl moiety, only occupying subsites S1 and S4. This correlates well with the IC_{50} potencies, where aloeresin D was approximately 3-fold less potent than aloesin (Fig. 3), and may indicate that the vinylphenol group of aloeresin D sterically hinders binding in the active site and in fact decreases the affinity of the ligand for M^{pro}. Removal and/or substitution of this group with smaller functional groups could result in more potent inhibitors that fit more snugly into the active site. In addition, removal of the vinylphenol ring of aloeresin D would likely change its Lipinski's rules of five parameters, decreasing the number of violations and improving its drugability. We also attempted to dock vitamin K, a natural product with structural similarity to anacardic acid, but did not obtain a binding pose that met the search criteria, likely due to the unsaturated, rigid hydrocarbon tail present in the vitamin K structure. While the *Aloe* compounds are not extremely potent inhibitors on their own, these results illustrate their potential as molecular scaffolds that can be further developed into more efficacious M^{pro} inhibitors. Furthermore, the excellent safety profile and bioavailability of both aloesin and aloeresin D make it likely that minor structural modifications to improve affinity to M^{pro} will not result in producing significant toxic liabilities. Given the limited number of validated chemical scaffolds currently available for M^{pro} inhibitors, identification of these compounds further adds to the medicinal chemist's toolkit for SARS-CoV-2 antiviral drug design.

In conclusion, here we have identified two natural product compounds, aloesin and aloeresin D, as novel SARS-CoV-2 M^{pro} inhibitors through screening of a high-content protease inhibitor library. Both of these compounds are safe in humans and have functional groups that are readily accessible for modification allowing them to serve as leads for M^{pro} inhibitors. Anacardic acid and TCID performed well in our study but were both ruled out due to potential toxicity. Additionally, we have confirmed that SARS-CoV-2 M^{pro} exhibits cooperative kinetics during catalysis, suggesting that the protein dimer interface may be an attractive target for allosteric inhibitors. Combined, these results advance our knowledge of structure–function relationships in M^{pro} and offer new molecular scaffolds for inhibitor design.

Declaration of competing interest

The authors declare that they have no known competing financial interests or personal relationships that could have appeared to influence the work reported in this paper.

Acknowledgements

The authors would like to gratefully acknowledge the invaluable assistance of Dr. Phil Reigan with helpful discussions and input. This work was supported by a faculty start-up grant generously provided by the University of Colorado, Skaggs School of Pharmacy and Pharmaceutical Sciences, Aurora, CO, USA. It should be noted that the University of Colorado, Skaggs School of Pharmacy and Pharmaceutical Sciences had no editorial input on the preparation of this manuscript or the planning, excitation, or interpretation of the experimental data.

Appendix A. Supplementary data

Supplementary data to this article can be found online at https://doi.org/10.1016/j.bmcl.2022.128732.

References

1 (CDC) USCfDC. Provisional Counts for Coronavirus Disease 2019 (COVID-19); 202https://www.cdc.gov/nchs/nvss/vsrr/covid19/index.htm. Accessed 12/05/21 2021.

2 University JH. Johns Hopkins Coronavirus Resource Center; 2021. https://coronavirus.jhu.edu/. Accessed 12/04/21 2021.

3 Burkert FR, Lanser L, Bellmann-Weiler R, Weiss G. Coronavirus disease 2019: clinics, treatment, and prevention. *Front Microbiol.* 2021;12, 761887.

4 Anjorin AA, Odetokun IA, Abioye AI, et al. Will Africans take COVID-19 vaccination? *PLoS ONE.* 2021;16, e0260575.

5 Sarwar A, Nazar N, Nazar N, Qadir A. Measuring vaccination willingness in response to COVID-19 using a multi-criteria-decision making method. *Hum Vaccin Immunother.* 2021::1–8.

6 Bergwerk M, Gonen T, Lustig Y, et al. Covid-19 Breakthrough Infections in Vaccinated Health Care Workers. *N Engl J Med.* 2021;385:1474–1484.

7 Hsu L, Grüne B, Buess M, et al. COVID-19 breakthrough infections and transmission risk: real-world data analyses from germany's largest public health department (Cologne). *Vaccines (Basel).* 2021;9.

8 Islam A, Ahmed A, Naqvi IH, Parveen S. Emergence of deadly severe acute respiratory syndrome coronavirus-2 during 2019–2020. *Virusdisease.* 2020;31:1–9.

9 Gazendam A, Nucci N, Ekhtiari S, et al. Trials and tribulations: so many potential treatments, so few answers. *Int Orthop.* 2020;44:1467–1471.

10 Gao K, Wang R, Chen J, Tepe JJ, Huang F, Wei GW. Perspectives on SARS-CoV-2 Main Protease Inhibitors. *J Med Chem.* 2021.

11 Boras B, Jones RM, Anson BJ, et al. Preclinical characterization of an intravenous coronavirus 3CL protease inhibitor for the potential treatment of COVID19. *Nat Commun.* 2021;12:6055.

12 Kundu D, Selvaraj C, Singh SK, Dubey VK. Identification of new anti-nCoV drug chemical compounds from Indian spices exploiting SARS-CoV-2 main protease as target. *J Biomol Struct Dyn.* 2021;39:3428–3434.

13 Ma C, Tan H, Choza J, Wang Y, Wang J. Validation and invalidation of SARS-CoV-2 main protease inhibitors using the Flip-GFP and Protease-Glo luciferase assays. *Acta Pharm Sin B.* 2021.

14 Al-Karmalawy AA, Farid MM, Mostafa A, et al. Naturally available flavonoid aglycones as potential antiviral drug candidates against SARS-CoV-2. *Molecules.* 2021;26.

15 Ma C, Xia Z, Sacco MD, et al. Discovery of Di- and trihaloacetamides as covalent SARS-CoV-2 main protease inhibitors with high target specificity. *J Am Chem Soc.* 2021.

16 Tsuji M. Potential anti-SARS-CoV-2 drug candidates identified through virtual screening of the ChEMBL database for compounds that target the main coronavirus protease. *FEBS Open Bio.* 2020;10:995–1004.

17 Ullrich S, Nitsche C. The SARS-CoV-2 main protease as drug target. *Bioorg Med Chem Lett.* 2020;30, 127377.

18 Weber IT, Wang YF, Harrison RW. HIV Protease: Historical Perspective and Current Research. *Viruses.* 2021;13.

19 Weichseldorfer M, Reitz M, Latinovic OS. Past HIV-1 medications and the current status of combined antiretroviral therapy options for HIV-1 patients. *Pharmaceutics.* 2021;13.

20 Pecoraro V, Banzi R, Cariani E, et al. New direct-acting antivirals for the treatment of patients with hepatitis c virus infection: a systematic review of randomized controlled trials. *J Clin Exp Hepatol.* 2019;9:522–538.

21 Zappulo E, Scotto R, Buonomo AR, Maraolo AE, Pinchera B, Gentile I. Efficacy and safety of a fixed dose combination tablet of asunaprevir + beclabuvir + daclatasvir for the treatment of Hepatitis C. *Expert Opin Pharmacother.* 2020;21:261–273.

22 Miao M, Jing X, De Clercq E, Li G. Danoprevir for the treatment of hepatitis C virus infection: design, development, and place in therapy. *Drug Des Devel Ther.* 2020;14:2759–2774.

23 Zhang L, Lin D, Sun X, et al. Crystal structure of SARS-CoV-2 main protease provides a basis for design of improved α-ketoamide inhibitors. *Science.* 2020;368:409–412.

24 Zhao W, Li X, Yu Z, Wu S, Ding L, Liu J. Identification of lactoferrin-derived peptides as potential inhibitors against the main protease of SARS-CoV-2. *Lebensm Wiss Technol.* 2022;154, 112684.

25 Bernardi M, Ghaani MR, Bayazeid O. Phenylethanoid glycosides as a possible COVID-19 protease inhibitor: a virtual screening approach. *J Mol Model.* 2021;27:341.

26 Arshia AH, Shadravan S, Solhjoo A, Sakhteman A, Sami A. De novo design of novel protease inhibitor candidates in the treatment of SARS-CoV-2 using deep learning, docking, and molecular dynamic simulations. *Comput Biol Med.* 2021;139, 104967.

27 Costanzi E, Kuzikov M, Esposito F, et al. Structural and biochemical analysis of the dual inhibition of MG-132 against SARS-CoV-2 main protease (Mpro/3CLpro) and human cathepsin-L. *Int J Mol Sci*. 2021;22.

28 Amin MR, Yasmin F, Hosen MA, et al. Synthesis, antimicrobial, anticancer, PASS, molecular docking, molecular dynamic simulations & pharmacokinetic predictions of some methyl β-D-galactopyranoside analogs. *Molecules*. 2021;26.

29 Citarella A, Scala A, Piperno A, Micale N. SARS-CoV-2 M(pro): a potential target for peptidomimetics and small-molecule inhibitors. *Biomolecules*. 2021;11.

30 Bahadur Gurung A, Ajmal Ali M, Al-Hemaid F, El-Zaidy M, Lee J. In silico analyses of major active constituents of Fingerroot (Boesenbergia rotunda) unveils inhibitory activities against SARS-CoV-2 main protease enzyme. *Saudi. J Biol Sci*. 2021.

31 Yan G, Li D, Lin Y, et al. Development of a simple and miniaturized sandwich-like fluorescence polarization assay for rapid screening of SARS-CoV-2 main protease inhibitors. *Cell Biosci*. 2021;11:199.

32 Baker JD, Uhrich RL, Kraemer GC, Love JE, Kraemer BC. A drug repurposing screen identifies hepatitis C antivirals as inhibitors of the SARS-CoV2 main protease. *PLoS ONE*. 2021;16, e0245962.

33 Chowdhury KH, Chowdhury MR, Mahmud S, et al. Drug repurposing approach against novel coronavirus disease (COVID-19) through virtual screening targeting SARS-CoV-2 main protease. *Biology (Basel)*. 2020;10.

34 Abdallah HM, El-Halawany AM, Sirwi A, et al. Repurposing of some natural product isolates as SARS-COV-2 Main Protease inhibitors via in vitro cell free and cell-based antiviral assessments and molecular modeling approaches. *Pharmaceuticals (Basel)*. 2021;14.

35 de Vera IM, Smith AN, Dancel MC, Huang X, Dunn BM, Fanucci GE. Elucidating a relationship between conformational sampling and drug resistance in HIV-1 protease. *Biochemistry*. 2013;52:3278–3288.

36 Bastys T, Gapsys V, Walter H, et al. Non-active site mutants of HIV-1 protease influence resistance and sensitisation towards protease inhibitors. *Retrovirology*. 2020;17:13.

37 King NM, Prabu-Jeyabalan M, Nalivaika EA, Schiffer CA. Combating susceptibility to drug resistance: lessons from HIV-1 protease. *Chem Biol*. 2004;11:1333–1338.

38 Iketani S, Forouhar F, Liu H, et al. Lead compounds for the development of SARS-CoV-2 3CL protease inhibitors. *Nat Commun*. 2021;12:2016.

39 Huff S, Kummetha IR, Tiwari SK, et al. Discovery and mechanism of SARS-CoV-2 main protease inhibitors. *J Med Chem*. 2021.

40 Ibbeson BM, Laraia L, Alza E, et al. Diversity-oriented synthesis as a tool for identifying new modulators of mitosis. *Nat Commun*. 2014;5:3155.

41 Gerry CJ, Schreiber SL. Chemical probes and drug leads from advances in synthetic planning and methodology. *Nat Rev Drug Discov*. 2018;17:333–352.

42 Moret N, Clark NA, Hafner M, et al. Cheminformatics tools for analyzing and designing optimized small-molecule collections and libraries. *Cell Chem Biol*. 2019; 26:765–777.e763.

43 Lipinski CA. Lead- and drug-like compounds: the rule-of-five revolution. *Drug Discov Today Technol*. 2004;1:337–341.

44 Lipinski CA, Lombardo F, Dominy BW, Feeney PJ. Experimental and computational approaches to estimate solubility and permeability in drug discovery and development settings. *Adv Drug Deliv Rev*. 2001;46:3–26.

45 Shilling PJ, Mirzadeh K, Cumming AJ, Widesheim M, Köck Z, Daley DO. Improved designs for pET expression plasmids increase protein production yield in Escherichia coli. *Commun Biol*. 2020;3:214.

46 Grum-Tokars V, Ratia K, Begaye A, Baker SC, Mesecar AD. Evaluating the 3C-like protease activity of SARS-Coronavirus: recommendations for standardized assays for drug discovery. *Virus Res*. 2008;133:63–73.

47 Akaike H. A new look at the statistical model identification. *IEEE Trans Autom Control*. 1974;19:716–723.

48 Panagiotopoulos AA, Karakasiliotis I, Kotzampasi DM, et al. Natural polyphenols inhibit the dimerization of the SARS-CoV-2 main protease: the case of fortunellin and its structural analogs. *Molecules*. 2021;26.

49 Davis DA, Bulut H, Shrestha P, et al. Regulation of the Dimerization and Activity of SARS-CoV-2 Main Protease through Reversible Glutathionylation of Cysteine 300. *mBio*. 2021;12, e0209421.

50 Shi J, Sivaraman J, Song J. Mechanism for controlling the dimer-monomer switch and coupling dimerization to catalysis of the severe acute respiratory syndrome coronavirus 3C-like protease. *J Virol*. 2008;82:4620–4629.

51 Cantrelle FX, Boll E, Brier L, et al. NMR spectroscopy of the main protease of SARS-CoV-2 and fragment-based screening identify three protein hotspots and an antiviral fragment. *Angew Chem Int Ed Engl*. 2021;60:25428–25435.

52 Jiménez-Avalos G, Vargas-Ruiz AP, Delgado-Pease NE, et al. Comprehensive virtual screening of 4.8 k flavonoids reveals novel insights into allosteric inhibition of SARS-CoV-2 M(PRO). *Sci Rep*. 2021;11:15452.

53 Sheik Amamuddy O, Afriyie Boateng R, Barozi V, Wavinya Nyamai D, Tastan BÖ. Novel dynamic residue network analysis approaches to study allosteric modulation: SARS-CoV-2 M(pro) and its evolutionary mutations as a case study. *Comput Struct Biotechnol J*. 2021;19:6431–6455.

54 Zhang JH, Chung TD, Oldenburg KR. A simple statistical parameter for use in evaluation and validation of high throughput screening assays. *J Biomol Screen*. 1999; 4:67–73.

55 Groom QJ, Reynolds T. Barbaloin in aloe species. *Planta Med*. 1987;53:345–348.

56 Aloes Manitto P. The Genus Aloe Edited by T. Reynolds (Jodrell Laboratory, Royal Botanical Gardens, Kew). CRC Press, Boca Raton, FL. 2004. xvii + 386 pp. 7 × 10 1/4 in. $119.95. ISBN 0-415-30672-8. *J Nat Prod*. 2005;68, 153-153.

57 Odes HS, Madar Z. A double-blind trial of a celandin, aloevera and psyllium laxative preparation in adult patients with constipation. *Digestion*. 1991;49:65–71.

58 Davis RH, Leitner MG, Russo JM, Byrne ME. Wound healing. Oral and topical activity of Aloe vera. *J Am Podiatr Med Assoc*. 1989;79:559–562.

59 Kim JH, Yoon J-Y, Yang SY, et al. Tyrosinase inhibitory components from Aloe vera and their antiviral activity. *J Enzyme Inhib Med Chem*. 2017;32:78–83.

60 Piao LZ, Park HR, Park YK, Lee SK, Park JH, Park MK. Mushroom tyrosinase inhibition activity of some chromones. *Chem Pharm Bull (Tokyo)*. 2002;50:309–311.

61 Gomes Júnior AL, Islam MT, Nicolau LAD, et al. Anti-inflammatory, antinociceptive, and antioxidant properties of anacardic acid in experimental models. *ACS Omega*. 2020;5:19506–19515.

62 Shan H, Liu J, Shen J, et al. Development of potent and selective inhibitors targeting the papain-like protease of SARS-CoV-2. *Cell Chem Biol*. 2021;28:855–865.e859.

63 Andra SS, Charisiadis P, Arora M, van Vliet-Ostaptchouk JV, Makris KC. Biomonitoring of human exposures to chlorinated derivatives and structural analogs of bisphenol A. *Environ Int*. 2015;85:352–379.

64 Trott O, Olson AJ. AutoDock Vina: improving the speed and accuracy of docking with a new scoring function, efficient optimization, and multithreading. *J Comput Chem*. 2010;31:455–461.